Laser and Particle Beams (2004), *22*, 245–251. Printed in the USA.
Copyright © 2004 Cambridge University Press 0263-0346/04 $16.00
DOI: 10.1017/S0263034604223060

X-ray spectral diagnostics for satellite lines of H-like Mg ions measured by a high resolution spectrometer

TAKAKO KATO,[1] NORIMASA YAMAMOTO,[2] AND FRANK B. ROSMEJ[3]
[1]National Institute for Fusion Science, Toki, Japan
[2]Rikkyo University, Tokyo, Japan
[3]Université de Provence et CNRS, Centre de Saint Jérôme, PIIM, UMR, Marseille cedex, France

(RECEIVED 1 November 2003; ACCEPTED 17 February 2004)

Abstract

X-ray spectra of H-like Mg ions produced in a laser plasma have been measured by space-resolved high-resolution spectroscopy. We identified satellite lines near Lyα lines, $2lnl' - 1snl' + h\nu$ for $n = 2$, 3, and 4. We construct a collisional radiative model including the doubly excited states for the intensity ratios of satellite lines. We use atomic data calculated by different methods for satellite lines and compare the results. We derive the electron temperature and density of the laser-produced plasma by a new technique using intensity ratios of only satellite lines. This technique is useful because the Lyα lines are often affected by opacity.

Keywords: H-like Mg ions; Plasma diagnostics; Satellite line; X-ray spectra

1. INTRODUCTION

In high temperature and high density plasmas, satellite lines emitted through doubly excited states are important for plasma diagnostics. Satellite lines have been widely used for plasma diagnostics of solar flares (e.g., Dubau & Volonte, 1980; Bely-Dubau *et al.*, 1982), Tokamak plasmas (e.g., Bitter *et al.*, 1984; Kato *et al.*, 1987), and laser-produced plasmas (Fujimoto *et al.*, 1981; Demir *et al.*, 1997), especially for dielectronic satellite lines of Li-like ions. In this article we study the satellite lines of He-like ions in detail. We have made a collisional-radiative model (CRM) for H-like and He-like ions including the doubly excited states. X-ray spectra of H-like Mg ions were measured from a laser-produced plasma with a high-resolution spectrometer by Rosmej *et al.* (1999, 2001). We identify satellite lines for $1snl$ lines ($n = 2$–4) and analyzed the spectra using our CRM. We compare three kinds of atomic data for spectral analysis. We derived temperatures of 180, 200, and 210 eV at three points imaged by the spectrometer. The derived electron density is 5×10^{20} cm^{-3}.

Address correspondence and reprint requests to: Takako Kato, Atomic and Molecular Data Research Center, Data and Planning Center, National Institute for Fusion Science, Oroshi-cho, Toki, Gifu, 509-5292, Japan. E-mail: kato.takako@nifs.ac.jp

2. EXPERIMENTAL SETUP

X-ray line spectra with high spectral resolution ($\lambda/\Delta\lambda \sim 5000$) were measured at the nhelix-laser facility at GSI-Darmstadt (Rosmej *et al.*, 1999, 2001). The laser is a 100-J Nd-glass laser ($\lambda = 1.046$ μm), with a pulse width of 15 ns and energy of 17 J. A massive Mg target is irradiated at normal incidence. The focal spot diameter on the target is 500 μm. X rays generated at the target are observed with a spherically bent mica crystal in second-order refraction providing simultaneous high spatial and spectral resolution. The mica crystal was used in order to have a spherical geometry for the Bragg crystal, which permit simultaneous high spectral and spatial resolution while maintaining high luminosity (because no slit is required for the space resolution). The second order was used to increase the resolution. In first order, the imaging properties of the spherical geometry are not so good because the Bragg angle is too small. The spatial resolution in the z-direction is 14 μm. Because X-ray film is used to record the spectra, there is no time resolution.

We have analyzed spectra from three different positions: "center," "+170 μm" and "−170 μm." The "center" position corresponds to the crossing points of the laser beam and the surface of the target. The "+170 μm" position corresponds to a position separated 170 μm from center in the normal direction. The "−170 μm" position corresponds to a

position below the center point. The observed spectra are shown in Figure 1.

3. COLLISIONAL-RADIATIVE MODEL FOR SATELLITE LINES

Normally collisional-radiative models (CRM) include only singly excited states, and the doubly excited states, which lie under a singly excited state, are not explicitly included. However we observe many satellite lines that are emitted through the doubly excited states in X-ray spectra from laser-produced plasmas, solar flares, and magnetic confined plasmas such as tokamak. We have constructed a CRM of the H-like and He-like system including the He-like doubly excited states including the $n = 2$ ($2s$ and $2p$) levels for H-like ions and the levels up to $n = 3$ ($3s$, $3p$, and $3d$) for H-like levels. Details of this model are given in Yamamoto *et al.* (2002) and Kato *et al.* (2001).

3.1. Energy level

In our CRM the ground state $1s^2$ and singly excited states $1snl$, doubly excited states $2l'nl$ and $3l'nl$ for He-like ions, and $1s$, $2l$, and $3l$ states for H-like ions are included. The total number of levels is 367: $1snl$ (60 states), $2l'nl$ (230 states), and $3l'nl$ (70 states). For singly excited states, $1snl$, $n = 2$ states are resolved in fine structure levels; for the states with $3 \leq n \leq 7$, the different total angular moment J states are combined keeping L and S separate; for the levels with $8 \leq n \leq 10$, the total orbital angular momentua L are combined but spin S are kept separate; and for the levels with $11 \leq n \leq 20$, they are averaged into the principal quantum number n. For doubly excited states, $2l'nl$, with $2 \leq n \leq 5$ are resolved into fine structure levels, and the levels with $6 \leq n \leq 20$ are combined into the averaged excited states as $1snl$ states. For doubly excited states, $3l'nl$, $n = 3$ levels are averaged with total angular moment J, and $4 \leq n \leq 20$ are averaged with orbital quantum number l. In Figure 2 the schematic energy level diagram for our CRM is shown.

3.2. Rate equation

An emission line intensity is calculated using a population density of an upper level multiplied by a radiative transition rate. Population densities are calculated by rate equations as follows:

$$\frac{dN_i}{dt} = -\sum_i W_{ii} N_i + \sum_j W_{ji} N_j, \tag{1}$$

where W_{ji} is a total transition rate from j state to i state.

Atomic processes considered in our model are electron impact excitation/de-excitation, ionization/three-body recombination, radiative recombination, and dielecronic capture, radiative transition, and autoionization. Collisional atomic data (excitation and ionization) for singly excited states $1snl$ and for doubly excited states $2l'nl$ are the same as used in Yamamoto *et al.* (2002). Collisional excitation rate coefficients between doubly excited states $2l2l'$ are taken from Goett *et al.* (1983) and from $1s2l$ to $2l'2l''$ are taken from Sampson *et al.* (1983). The transition rates between doubly excited states $3l'nl$ are calculated using the HULLAC code (Bar-Shalom *et al.*, 1988).

Eq. (1) is solved assuming quasi-steady state for doubly and singly excited states. Under this assumption we can write the steady-state population densities N_i of excited states as a linear combination of the population densities of $1s^2$, $1s$, $2s$, $2p$, $3s$, $3p$, and $3d$ as follows:

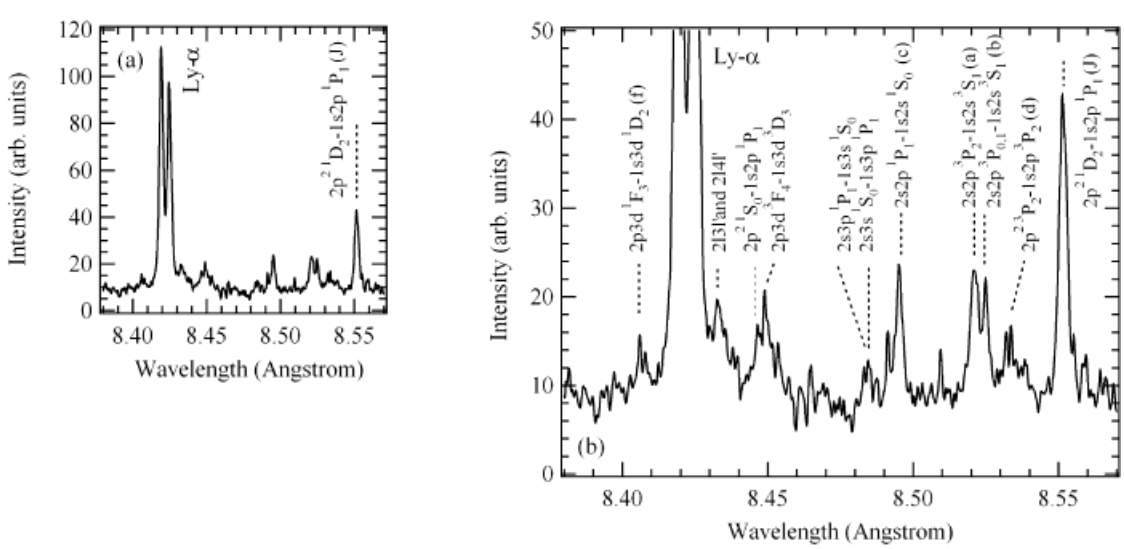

Fig. 1. a: The measured spectrum near H-like Mg Lyα lines. The spectrum is obtained from "center." b: The measured spectrum near Lyα lines with identification for satellite lines.

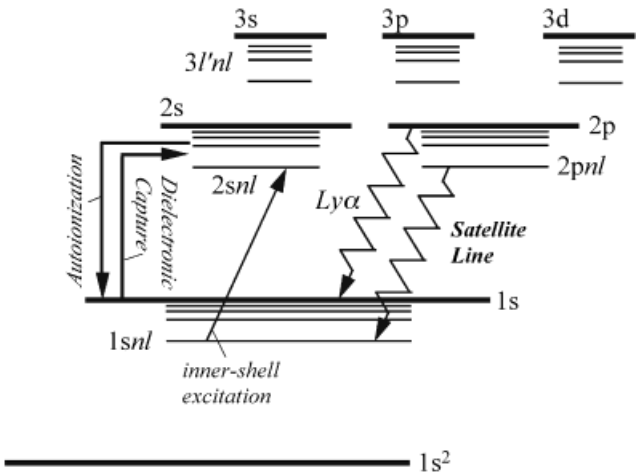

Fig. 2. The schematic energy level diagram for our CRM.

$$N_i = \sum_y r_i^y N_e N_y, \tag{2}$$

where r_i^y and N_e are the population density coefficient and the electron density, respectively. The suffix y indicates the ground states of He-like ions $1s^2$ and H-like ions $1s$, and H-like excited states, $2s$, $2p$, $3s$, $3p$, and $3d$.

Line intensities are then obtained by multiplying the population density N_i, and radiative transition rate A^r as follows:

$$I_s = N_i A^4. \tag{3}$$

3.3. Discussion of the averaged level model for satellite line spectra

When we have to take into account many excited states in CRM, we can consider the averaged levels for simplicity. In an averaged level model, the population densities of detailed levels are obtained distributing the averaged level population density according to the statistical weights. Then the line intensities for detailed levels are calculated from the population densities in averaged model. We find the difference in satellite line intensities between an averaged model (the level with different J but with the same configuration is combined to one level) and an individual level model (the levels are separated with J) separated with fine structure levels. Comparison with an averaged model described in Yamamoto *et al.* (2002) and Kato *et al.* (2001) and an individual model calculated in this article is discussed in this section. Both models use atomic data from the MZ code (Vainshtein & Safronova, 1978, pers. comm., 2000). Comparisons for satellite line spectra by two different models are shown in Figure 3 for (a) $1s3l$–$2l3l'$, (b) $1s3l$–$2l4l'$ and (c) $1s3l$–$2l5l'$. To avoid the density effect on line intensities, electron density in the calculation is assumed to be 1 cm^{-3}, which corresponds to the low-density limit.

The averaged model assumes the population densities are proportional to the statistical weights of the levels. There-

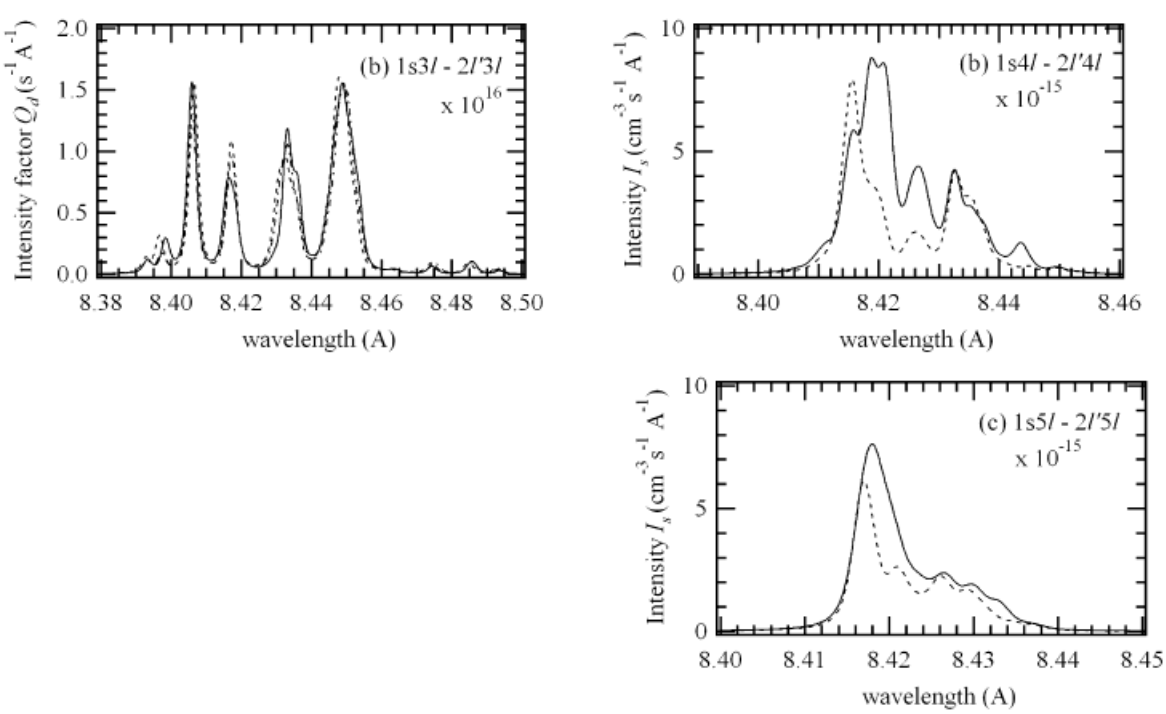

Fig. 3. Comparison of satellite line spectra between models with averaged levels (solid line) and individual levels (dotted lines). Electron and ion temperatures are assumed to be 200 eV and 180 eV, respectively. Electron density N_e is assumed to be 1 cm^{-3}, and the instrumental width is taken to be 1.5 mÅ. a: $1s3l$–$2l'3l$; b: $1s4l$–$2l'4l$; and c: $1s5l$–$2l'5l$ transitions.

fore, generally, the intensities by an averaged model give larger intensities than the individual model in total. We can say that the intensities in an averaged model correspond to those in a high density limit where the collisional processes are dominant.

Comparison between averaged and individual models for $1s3l$–$2l'3l$ transitions are shown in Figure 3a. Between 8.38 Å and 8.50 Å, satellite line intensities by the averaged model are larger than those by the individual model except line f ($1s3d\ ^1D_2$–$2p3d\ ^1F_3$, 8.406 Å). In the averaged model three $2p3d$ singlet levels (^1P, ^1D, and ^1F) are combined into one $2p3d$ singlet level. Because the autoionization rate for $2p3d\ ^1F_3$ is larger than those of other $2p3d\ ^1P$, ^1D levels, the population density of $2p3d\ ^1F$ become smaller in the averaged model compared to an individual model. When the electron temperature is derived from the intensity ratio I_f/I_J, the predicted temperature might be overestimated in an averaged model. In the wavelength range of 8.46–8.48 Å, disagreement of spectra is due to the effect of the averaged $2p3p$ levels. Because the autoionization rate for $2p3p\ ^3D$ is small, the population density in an individual model is small. However in the averaged model the population density becomes large due to the effect of other $2p3p$ levels where the dielectronic capture rates are large. For $1s4l$–$2l'4l$ transitions, in the wavelength range longer than 8.43 Å, the agreement between the two models is good. However, the spectra from the averaged model in the range 8.41–8.43 Å is larger than that from the individual model by a factor of 2–3 as shown in Figure 3b. The line intensities between 8.4157–8.4158 Å are stronger from the individual model than from the averaged model because the autoionization rates from $2p4f\ ^3D$, the upper levels for these transitions, are large compared to other $2p4f$ triplet levels.

4. ATOMIC DATA

To interpret the observed spectra, atomic data are very important. We compare here three different theoretical data sets calculated using (1) MZ code by Vainshtein and Safronova (1978) and U.I. Safronova (pers. comm.), Vinogradov *et al.* (1975), (2) a code based on relativistic many-body perturbation theory combined with complex rotation by Lindroth (MBL; Tokman *et al.*, 2002), and (3) a code based on relativistic many-body perturbation theory by Safronova (MBS; pers. comm.).

We compare the atomic data for satellite lines $1s2l$–$2l'2l$, $1s3l$–$2l'3l$, $1s4l$–$2l'4l$, and $1s5l$–$2l'5l$. Three atomic data sets by MZ, MBS, and MBL are compared for the wavelengths, radiative transitions, autoionization rates, and intensity factor Q_d:

$$Q_d = \frac{g_i A^r A^a}{\sum A^r + \sum A^a}, \tag{4}$$

where g_i is a statistical weight for upper state i, A^r is the radiative transition rate from level i to j, and A^a is the autoionization rate from level i. The data by MZ are represented by the LS coupling scheme and those by MBS and MBL are jj coupling. Generally for $2l2l'$ and $2l3l'$ lines, agreements are good. Large differences are found for $2l4l'$ and $2l5l'$ lines between MZ and many body theory (MBS and MBL). In the following, the differences in atomic data are represented by percentages relative to the values given by the MZ method (e.g., $(\mathrm{MBS} - \mathrm{MZ})/\mathrm{MZ} \times 100$).

Comparison of the different atomic data, MZ, MBS, and MBL, is given in Figure 4 for (a) $n = 2$, (b) $n = 3$, (c) $n = 4$, and (d) $n = 5$ transitions in a form of convoluted intensity factor, $Q_d \times P(\lambda)$, where $P(\lambda)$ is a line profile of Voigt type.

Most of the data for $1s2l$–$2l'2l$ transitions, the A^a and A^r values agree within ±20%. The difference in intensity factor Q_d for these transitions is about 10%. The largest difference for A^a values is 30% for the $2p^2\ ^3P_2$ state, which is the upper state of line d. The disagreement in Q_d for d line is also 30% for both MBS and MBL data. For J line ($1s2p\ ^1P_1$–$2p^2\ ^1D_2$), which has the largest A^a in satellite lines, wavelength of MBS is 1.6 mÅ shorter than MZ and MBL.

The difference for $1s3l$–$2l'3l$ transitions are larger than those for $1s2l$–$2l'2l$ transitions. The differences of A^a for $2p3d\ ^1F_3$, the upper level of line f, are 40% for MBS and 5% for MBL, and the differences of Q_d are 13% for MBS and −7% for MBL, respectively. The strongest line in this wavelength range is $1s3d\ ^3D_3$–$2p3d\ ^3F_2$ and the atomic data for this transition agree well.

The discrepancies for $1s4l$–$2l'4l$ transitions are much larger than those for $n = 2$ and 3. Especially, A^a values by MZ for $2p4f\ ^3D_{1,2,3}$, which are the upper states of satellite lines in the wavelength range of 8.4157–8.4158 Å are larger by 1–4 orders of magnitude than those by MBS and MBL. Therefore, Q_d values of these transitions by MZ are also larger by a factor of 10–10^3 than MBS and MBL.

For $n = 5$ transitions, Q_d values of transitions from the upper states $2s5f\ ^3F$ and $2p5f\ ^3D$ by MBL are smaller by a factor of 10–10^3 than those by MZ, because the autoionization rates by MBL are smaller than MZ by a factor of 10^2–10^4. Therefore the large difference is found at around 8.417 Å as shown in Figure 4d. The Q_d value for $1s5d\ ^3D_3$–$2p5d\ ^3F_4$ (8.426 Å) transition by MBL is 20% of that by MZ because the autoionization rate is about 20% and the radiative transition rate is 30% of those by MZ.

5. PLASMA DIAGNOSTICS FOR T_e AND N_e USING SATELLITE LINE INTENSITY RATIOS

Because the satellite line intensities depend on electron temperature T_e and density N_e, the satellite line intensity ratios depend on T_e and N_e. The intensities in this section are calculated for an ionizing plasma where the doubly excited states are populated by dielectronic capture from the $1s$ state only.

The density dependence is mainly caused by the collisional process through l-changing with the same quantum number n. Electron density dependence for several line

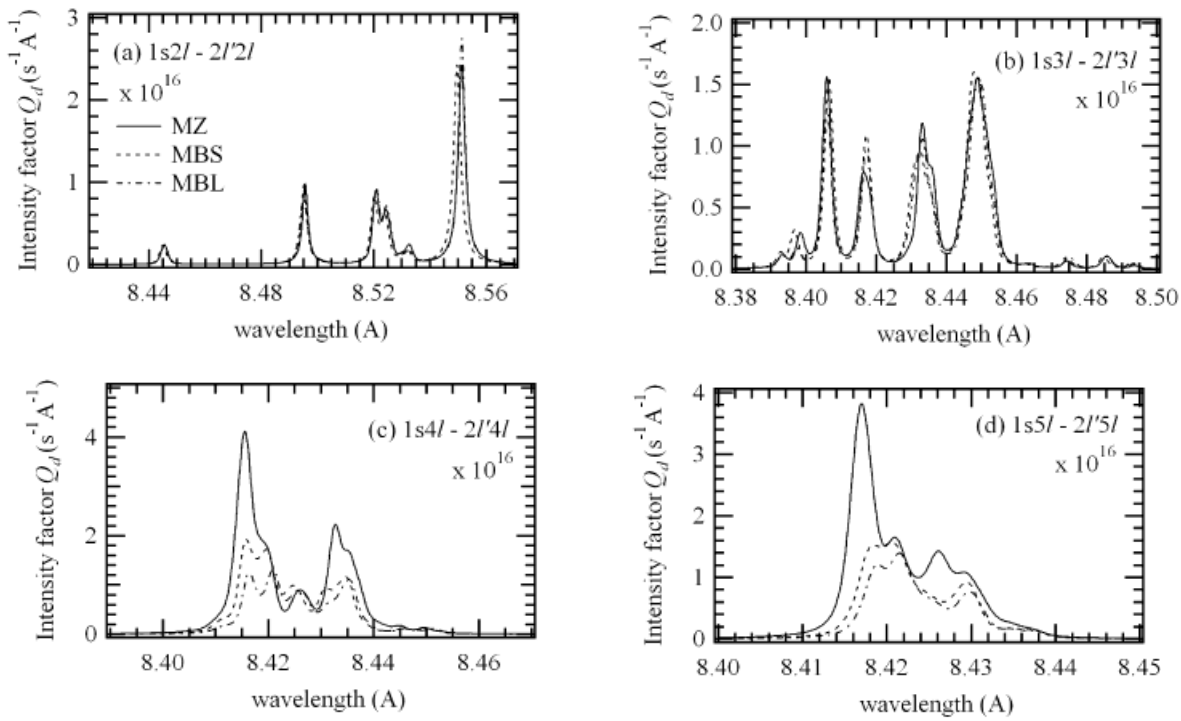

Fig. 4. Comparison of intensity factor convoluted by the Voigt profile function for three different atomic data sets by MZ (solid line), MBS (dotted line), and MBL (dot-dashed line). Ion temperature T_i = 200 eV and instrumental width 1.5 mÅ are assumed. a: $1s2l$–$2l'2l$; b: $1s3l$–$2l'3l$; c: $1s4l$–$2l'4l$; and d: $1s5l$–$2l'5l$ transitions.

intensity ratios of satellite lines at $T_e = 200$ eV are shown in Figure 5 as calculated by two different atomic data sets, MZ and MBL. Among intensity ratios, $I_d\,(1s2p\ ^3P_2$–$2p^2\ ^3P_2)/I_J\,(1s2p\ ^1P_1$–$2p^2\ ^1D_2)$ has a strong dependence as shown in Figure 5. Because the dielectronic capture rate to $2s2p\ ^3P_2$ is larger than that of $2p^2\ ^3P_2$ by a factor of 5, the population densities of these states are $N\,(2s2p\ ^3P_2) > N\,(2p^2\ ^3P_2)$ at low densities. With increasing electron density, population density of $2p^2\ ^3P_2$ increases by l-changing collisional excitation from the $2s2p\ ^3P_2$ state [12]. On the contrary, the population density $2s2p\ ^3P$ is decreased by l-changing collisions. Therefore the ratio $I_d(1s2p\ ^3P_2$–$2p^2\ ^3P_2)/I_J(1s2p\ ^1P_1$–$2p^2\ ^1D_2)$ increases with increasing density for $N_e \geq 10^{19}$ cm^{-3} and the ratio of $I_a(1s2s\ ^3S_1$–$2s2p\ ^3P_2)/I_J(1s2p\ ^1P_1$–$2p^2\ ^1D_2)$ gradually decreases over $N_e = 10^{20-21}$ cm^{-3}. The ratio $I_f(1s3d\ ^1D_2$–$2p3d\ ^1F_3)/I_J(1s2p\ ^1P_1$–$2p^2\ ^1D_2)$ also decreases at higher densities than 10^{21} cm^{-3}. On the other hand, the ratio $I_c(1s2s\ ^1S_0$–$2s2p\ ^1P_1)/I_J(1s2p\ ^1P_1$–$2p^2\ ^1D_2)$ has no dependence on electron density. The intensity ratio I_d/I_J can be used for electron density diagnostics in the electron density range $N_e \geq 10^{20}$ cm^{-3}. Electron density derived from I_d/I_J by MBL gives larger values than that by MZ.

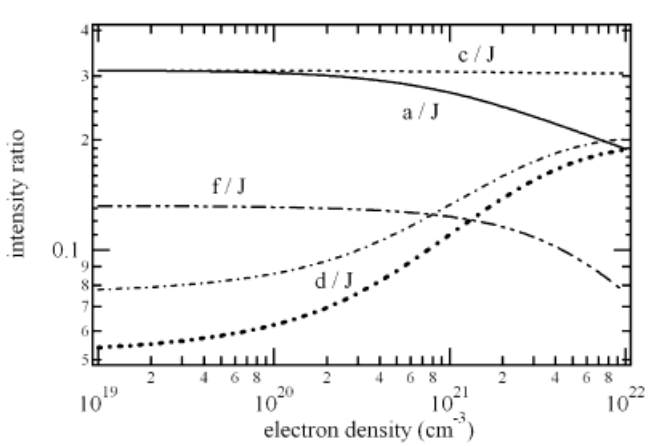

Fig. 5. Density dependence of theoretical line intensity ratio at $T_e = 200$ eV in an ionizing plasma. Thin lines are intensity ratios by MZ for I_a/I_J (solid line), I_c/I_J (dotted line), I_d/I_J (dot-dashed line), and I_f/I_J (dot-dot-dashed lines). Bold dot dashed line is for I_d/I_J by MTL.

Electron temperature dependence of several line intensity ratios at $N_e = 10^{20}$ cm^{-3} are shown in Figure 6. The ratio $I_J/I_{Ly\alpha}$ strongly decreases with increase of temperature. The intensity ratios of the satellite lines to the resonance line have been often used to estimate electron temperature in high temperature plasmas (e.g., Kaot *et al.*, 1998). However in our case we do not use this ratio because Lyα might be affected by opacity as mentioned in Section 2. The intensity ratios of lines, which have the same n quantum number as an upper state, have no temperature dependence. The line intensity ratios with different quantum numbers n as upper states such as, I_f/I_J can be used to estimate temperature, although dependence on temperature of intensity ratio I_f/I_J is much weaker than $I_J/I_{Ly\alpha}$. On the contrary, independence of tem-

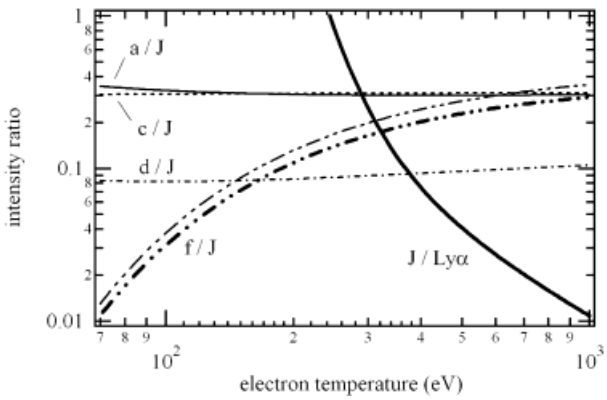

Fig. 6. Temperature dependence of theoretical line intensity ratio at $N_e = 10^{20}$ cm^{-3} in an ionizing plasma. Bold solid line is for $I_J/I_{Ly\alpha}$. Thin lines are intensity ratios by MZ for I_a/I_J (solid line), I_c/I_J (dotted line), I_d/I_J (dot-dashed line), and I_f/I_J (dot-dot-dashed lines). Bold dot dot dashed line is for I_f/I_J by MBL.

perature and density for the ratio I_c/I_J can be used to define a reference line ratio in the measured spectra.

6. SPECTRAL ANALYSIS

We analysed three kind of spectra measured from center, -170 μm, and $+170$ μm. The intensity ratio I_f/I_J has a strong temperature dependence and I_d/I_J has density dependence as shown in Section 5. We used mainly these two intensity ratios to derive the electron temperature and density. Among three sets of atomic data compared in Section 4, we used MZ and MBL data for our spectral analysis and compared the derived plasma parameters. The satellite line intensities are calculated by our collisional radiative model including the dielectronic states. Ionization equilibrium is assumed in our analysis.

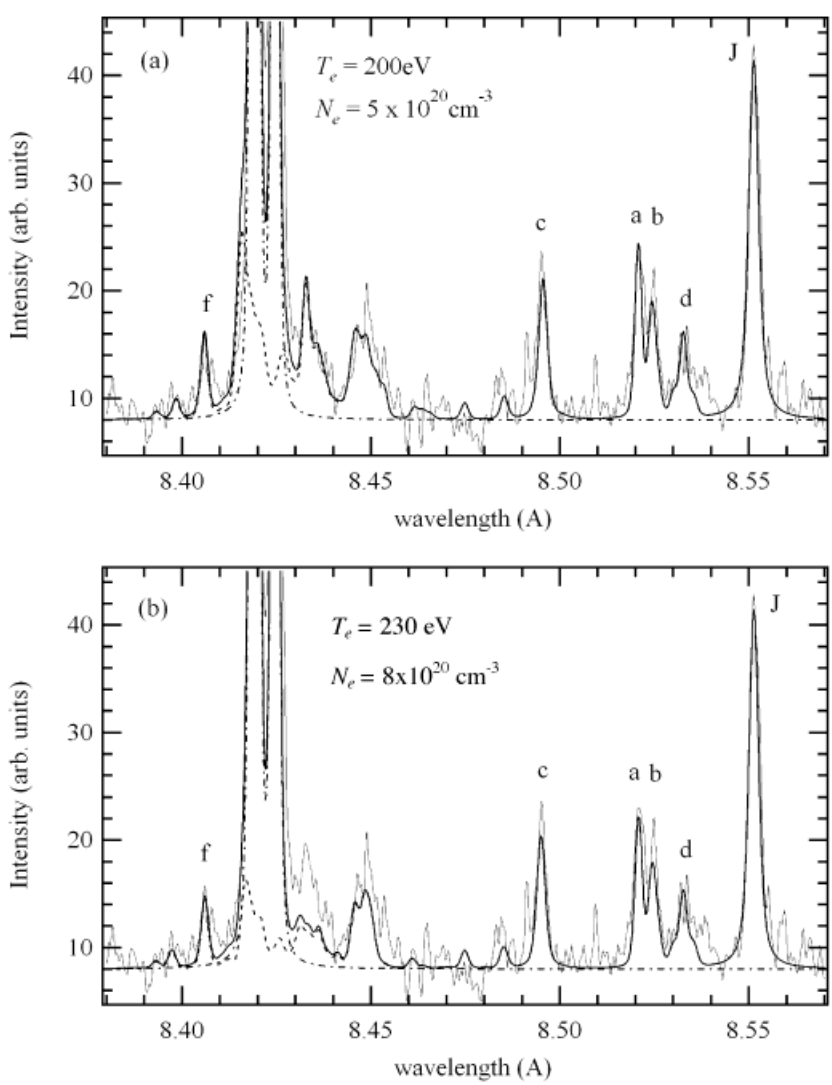

Fig. 7. The observed (thin line) and theoretical spectra (bold lines) from "center." Solid, dashed, and dot-dashed lines are the sum of satellite lines and Lyα, the sum of all the satellite lines $1snl$–$2l'nl$ (n = 2, 3, 4, and 5), Lyα lines. Instrumental width w is 0.5 mÅ. a: With atomic data by MZ. T_e = 200 eV, T_i = 200 eV, and $N_e = 5 \times 10^{20}$ cm^{-3}. b: With atomic data by MBL. T_e = 230 eV, T_i = 220 eV, and $N_e = 8 \times 10^{20}$ cm^{-3}.

Theoretical spectra using the atomic data by MZ and MBL are shown by dotted lines in Figure 7a, b, respectively. In the MZ case, the electron density N_e is obtained approximately 5×10^{20} cm^{-3} from the intensity ratio of I_d/I_J. The temperature $T_e = 200$ eV is derived from the intensity ratio I_f/I_J with MZ atomic data. This temperature corresponds to the high temperature limit to fit the spectra in the wavelength range near the foot of Lyman α. When we use the atomic data by MBL, the derived temperature $T_e = 230$ eV, which is higher than that by MZ because of the difference of atomic data for the *f* line. Two broad peaks near 8.43–8.44 Å and 8.44–8.46 Å are consistent with a large number of weak satellite lines, not only from $2l3l'$ but also $2l4l'$ and $2l5l'$. They are in good agreement with the measured spectra in the case of MZ. On the shorter wavelength side of Lyman α (~8.415 Å) the calculated spectrum exceeds the measured spectrum as seen in Figure 7a. This excess comes mainly from $1s4f$–$2p4f$ lines, which are much stronger by MZ than MBL, as discussed in Section 4. Theoretical spectral feature near Lyman α foot with MBL atomic data agrees with the measured spectra better than that by MZ. Although the satellite lines in 8.44–8.46 Å are in good agreement, the theoretical spectra in 8.43–8.44 Å is too small in the case of MBL. The line intensity ratio I_c/I_J does not depend on temperature and density and should be constant for any condition, as shown in Figures 5 and 6. This intensity ratio can be used to determine the background level. We derived the background level considering the intensity ratio of I_c/I_J. However as seen in Figure 7, the theoretical intensity of line *c* is always smaller than the observed intensity. The atomic data for *c* might be wrong or there is some dynamic effects in plasma. The ion temperature is assumed to be $T_i = 200$ eV for the theoretical spectra. This value is derived from the observed line profile of *J* and *c*.

For the spectra of -170 μm, we obtained $T_e = 180$ eV and $N_e = 4 \times 10^{20}$ cm by MZ data. For the spectra of $+170$ μm, we derived $T_e = 210$ eV and $N_e = 5 \times 10^{20}$ cm^{-3} as a best fit with atomic data by MZ.

7. SUMMARY AND DISCUSSION

We have constructed CRM including doubly excited states and analyzed X-ray spectra of H-like Mg ions measured at GSI. We identified satellite lines for $2l2l'$, $2l3l'$ and $2l4l'$ transitions from the measured spectra.

We study the density and temperature dependences of satellite line intensity ratios. We proposed the new method for plasma diagnostics using only satellite line intensity ratios. We compared three kinds of atomic data, MZ, MBL, and MBS for spectral analysis. We found a better spectral fit with MZ data than MBT in 8.43–8.44 Å ($2l4l'$ lines). However MBT is better than MZ near 8.415 Å ($2l5l'$ lines).

The plasma parameters are derived with the satellite line intensity ratios. The derived parameters are $T_e = 200 \pm 10$ eV and $N_e = 5 \pm 2 \times 10^{20}$ cm^{-3} for the center position, $T_e = 210$ eV and $N_e = 5 \times 10^{20}$ cm^{-3} for $+170$ μm, and $T_e = 180$ eV and $N_e = 4 \times 10^{20}$ cm^{-3} for -170 μm.

We are going to analyze the spectra including the intensity of Lyα lines with the effect of opacity using Monte Carlo simulation. We would like also to study the dynamic effect on the observed spectra.

REFERENCES

Bar-Shalom, A., Klapsch, M. & Oreg, J. (1988). *Phys. Rev. A* **38** 1773.

Bely-Dubau, F., Dubau, J., Faucher, P., Gabriel, A.H., Loulergue, M., Steenman-Clark, L., Volonte, S., Antonucci, E. & Rapley, C.G. (1982). *Mom. Not. R. Astron. Soc* **201**, 1155.

Bitter, M. *et al.* (1984). *Phys. Rev. A* **29**, 661.

Demir, A., Zeitoun, P., Tallents, G.J. *et al.* (1997). *Phys. Rev. E* **55**, 1827.

Dubau, J. & Volonte, S. (1980). Dielectronic recombination and its applications in astronomy. *Rep. Prog. Phys.* **43**, 199–251.

Fujimoto, T., Yamaguchi, N., Mizui, J., Kato, T. & Fujita, F. (1981). *J. Phys. D* **14**, 439.

Goett, S.T., Sampson, D.H. & Clark, R.E.H. (1983). *Atomic and Nuclear Data Table* **28**, 279.

Kato, T., Fujiwara, T. & Hanaoka, Y. (1998). *Astrophys. J.* **492**, 822–832.

Kato, T., Morita, S., Masai, K. & Hayakawa, S. (1987). *Phys. Rev. A* **36**, 795–803.

Kato, T., Yamamoto, N., More, R. & Fujimoto, T. (2001). *J Quantitative Spectroscopy and Radiative Transfer* **71**, 431.

Rosmej, F.B. *et al.* (1999). *JETP Lett.* **70**, 270.

Rosmej, F.B. *et al.* (2001). *Phys. Rev. A* **63**, 32716.

Sampson, D.H., Goett, S.J. & Clark, R.E.H. (1983). *ADNDT* **28**, 299.

Tokman, M., Eklöw, N., Glans, P., Lindroth, E., Schuch, R., Gwinner, G., Schwalm, D., Wolf, A., Hoffknecht, A., Müller, A. & Schippers, S. (2002). *Phys. Rev. A* **66**, 012703.

Vainshtein, L.A. & Safronova, U.I. (1978). *ADNDT* **25**, 311.

Vainshtein, L.A. & Safronova, U.I. (2000). personal communication.

Vinogradov, A.V., Skobelev, I.Yu., Yukov, E.A. (1975). *Sov. J. Quant. Electron.* **5**, 630.

Yamamoto, N., Kato, T. & Fujimoto, T. (2002). *J. Plasma Fusion Res.* **78**, 193.